# Carbon Nanofiber Aerogel/Magnetic Core-Shell Nanoparticle Composites as Recyclable Oil Sorbents

Pimchanok Ieamviteevanich[1], Dulyawich Palaporn[1], Narong Chanlek[2], Yingyot Poo-arporn[2], Wiyada Mongkolthanaruk[3], Stephen J. Eichhorn[4], Supree Pinitsoontorn[1, 5*]

[1]*Materials Science and Nanotechnology Program, Department of Physics, Faculty of Science, Khon Kaen University, Khon Kaen 40002, THAILAND.*

[2]*Synchrotron Light Research Institute (Public Organization), 111 University Avenue, Muang District, Nakhon Ratchasima 30000, Thailand.*

[3]*Department of Microbiology, Faculty of Science, Khon Kaen University, Khon Kaen 40002, THAILAND.*

[4]*Bristol Composites Institute, CAME School of Engineering, University Walk, University of Bristol, Bristol, UK.*

[5]*Institute of Nanomaterials Research and Innovation for Energy (IN-RIE), NANOTEC-KKU RNN on Nanomaterials Research and Innovation for Energy, Khon Kaen University, Khon Kaen 40002, THAILAND.*

Corresponding author's email address: psupree@kku.ac.th

## Abstract

Developing sorbent materials for the removal of oil spills has become an attractive research topic in recent years for its impact on environmental and ecological concerns. The sorbents should be light, low cost, oil selective, environmentally friendly, mechanically robust, easily collected and recyclable, as well having high absorption capacities. Here, magnetic carbon nanofiber (MCF) aerogels have been developed from bacterial cellulose-based nanocomposites as efficient and recyclable oil sorbents. The MCF aerogels comprise a 3D interconnected structure of carbon nanofibers, with very high porosity, decorated with uniformly dispersed magnetic nanoparticles (NPs), with an Fe/$Fe_3O_4$ core-shell structure. The MCF aerogels exhibit very high magnetization (>100 emu $g^{-1}$), compared to other previously reported magnetic aerogels, due to the Fe core/$Fe_3O_4$ shell NPs, but additionally with an ultralow density of only ~7 mg $cm^{-3}$. Furthermore, the MCF aerogel is highly compressible up to 90% strain and instantly returns to the original shape after release without any plastic deformation. It is also highly durable, up to 100 compressive stress-strain cycles. As for oil sorbents, the MCF aerogel can absorb oils directly without any post-surface treatment, due to its hydrophobic/oleophilic property. The absorption capacities are in the range

of 37-87 g/g for various types of oils and organic solvents. These values are comparably large amongst magnetic carbon aerogels. Additionally, due to their large magnetization, the MCF aerogels can be easily manipulated during oil absorption and collected via external magnetic fields, which is beneficial for avoiding direct contact with possible hazardous solvents. They can then be recycled several times by dissolution with hardly any reduction in absorption capacity. This work has demonstrated that environmentally friendly biomass-derived MCF aerogels could be candidates for the absorption and recycling of oils and organic solvents from wastewater.

**Keywords:** bacterial cellulose; carbon nanofiber; aerogel; magnetic; oil absorption;

## Introduction

Oil pollutants and oil spills are one of many global concerns for their detrimental effects on the environment and their ecological impact. Frequent oil-spill accidents during exploration and transportation have caused catastrophic effects on marine ecosystems.[1] It is estimated that annual spillages of petroleum compounds to the global marine environment are in excess of 1.4 million tons.[2] A variety of methods and technologies have been applied to oil-spill remediation, such as chemical approaches, *in situ* burning, bioremediation, and mechanical recovery.[3] Among these methods, the use of sorbent materials is considered to be one of the most effective approaches because of their low cost, high selectivity, environmental friendliness, fast performance, good recyclability, and the possibility of complete oil removal.[3-5]

There are several types of sorbents for oil-spill remediation, such as polydimethylsiloxane (PDMS) sponge, polyurethane (PU) sponge, or melamine foam (MF), with some surface functionalization to increase the hydrophobic/oleophilic properties. For example, Du *et al.* decorated a commercial MF with cobalt nanodots, carbon nanotubes (CNT) and CoOH sheets, to create a microscopic hierarchical dimensional structure, which was further coated with PDMS to increase superhydrophobicity.[6] The modified MF exhibited large contact angles >160° and very high absorption capacities (50-145 g/g) over a wide range of oils and organic solvents. Chen *et al.* fabricated ultralight magnetic foams from a commercial PU sponge by chemical modification, and functionalization with magnetic ions before pyrolysis at 400 °C.[7] The magnetic foams, treated with methyltrichlorosilane to enhance superhydrophobic properties, demonstrated a high oil absorption

capacity up to 100 times the foams' weight, and could be easily recovered by magnetic extraction. Alternatively, oil sorbent materials can be produced from electrospun nanofibrous polymer composites.[8] For instance, Deuber *et al.* fabricated hierarchically structured pullulan/polyvinyl alcohol (PVA) aerogels by electrospinning, homogenizing, solid templating, and freeze-drying, respectively.[9] The aerogels, surface-modified with trichloro(octyl)silane, enabled rapid liquid uptake, additionally with a high liquid holding capacity.

In recent years, carbon-based materials have received attention from a number of research groups as oil sorbents or oil/water separators, due to their intrinsic hydrophobic properties, low density, and chemical stability.[3,5] In particular, carbon-based materials with three-dimensional (3D) architectures have received great interest due to their outstanding properties. These properties include bulky macroscopic shapes (for ease of collection without causing additional contamination), large surface areas, and high porosities.[4] Although CNT-based[10] and graphene sponges[11] are highly efficient for oil absorption (absorption capacities of several hundred times their weights), their fabrication requires expensive precursors and complex equipment which limits mass production. Pyrolysis of biomass is an effective and simple approach to produce low-cost carbon-based oil sorbents. Several biomass sources, including cotton,[12] winter melon,[13] poplars catkins,[14], popcorn,[15] bamboo,[16] and bacterial cellulose (BC),[17] containing a large proportion of cellulose, have been converted into 3D carbon aerogels *via* carbonization under an inert atmosphere. Oil/organic solvent absorption studies show that absorption capacities of these materials ranged from around 10-50 times their weight (for carbonized popcorn or winter melon)[13,15] to more than 150 times their weight (carbonized cotton or BC),[12,17] depending on the raw materials, fabrication processes, and types of liquid. Moreover, 3D carbon aerogels have been prepared from waste paper as an efficient and recyclable sorbent for oil and organic solvents.[18-19]

On the other hand, superhydrophobic surface-based magnetic materials have emerged for a range of potential applications, including oil spill capture and separation.[20] Traditionally, magnetic particles, ranging from micro- to nano- sizes, with a surface-modified core-shell structures, have been widely used.[21-23] The magnetic core provides controllability of the particle motion as well as the retraction of the powders by external magnetic fields, while the superhydrophobic shell enhanced oil adsorption. However, there are some unavoidable challenges when magnetic particles are applied in practical applications, such as the agglomeration of particles, the low oil absorption capacity, and the difficulty of complete retrieval, especially when

used on a large scale.[24] 3D porous carbon aerogels, with intrinsic hydrophobic properties, combined with magnetic particles, have been proposed. These materials can address nearly all the above issues. For example, Turco *et al.* fabricated a magnetically microporous PDMS/CNT nanocomposite *via* a low-cost approach, which is highly reusable and can be magnetically actuated by a relatively low magnetic field.[25] Cotton has also been carbonized and then immersed in an iron ion solution before pyrolysis to produce magnetic carbon nanofiber (CNF) aerogels.[26-27] Apart from the high efficiency for oil/water separation, cotton-derived CNF aerogels can be easily attracted by a magnetic force, providing a facile and energy-saving method to collect oils from polluted areas.

Bacterial cellulose (BC) is a class of nanocellulose produced from the cultivation of bacteria.[28] BC has been extensively studied as a potential oil sorbent by either surface modification of BC aerogels,[29-30] or pyrolysis to obtain 3D CNF aerogels. Sai *et al.* applied a trimethylsilylation process to modify the surfaces of BC aerogels.[29] The modified BC aerogels exhibited hydrophobic/oleophilic properties with high absorption capacities (86-185 g/g) for a wide range of organic solvents and oils.[29] On the other hand, pioneering work by Wu *et al.* reported ultralight, flexible, and fire-resistant CNF aerogels from the pyrolysis of BC.[17] The density of the CNF aerogels was only 4-6 mg $cm^{-3}$, and the absorption efficiency was very high (up to 300 times its weight) for various kinds of organic solvents and oils. Furthermore, Lai *et al.* fabricated carbon aerogels consisting of one-dimensional CNF derived from BC and a 3D carbon skeleton derived from polyimide (PI).[31] These materials were considered as potentially versatile adsorbents, as well as supercapacitor electrodes.[31] In addition, the carbonized BC aerogels comprising graphene,[32] or graphene oxide[33] were found to exhibit superior oil absorption capacities (up to several hundred times their weight) compared to most previously reported carbon-based sorbents. The ultrahigh absorption capacity was ascribed to the low density and high porosity of the composite CNF aerogels.[32-33]

Magnetic nanoparticles (NPs) have been incorporated in BC-derived CNF aerogels by several means to enable synergistic advantages. Several choices of magnetic particles are available, such as Co,[34] $CoFe_2O_4$,[35] and NiCo[36]. The most popular materials are however iron oxides ($Fe_2O_3$,[37] $Fe_3O_4$[38-41]) due to their strong magnetization and chemical stability. These CNF/NP systems have been considered for potential applications in various fields, such as catalysts,[34-35] lithium-ion batteries,[41] and electromagnetic shielding.[36,38-40] In this work, BC

aerogels were magnetically functionalized by co-precipitation of $Fe_3O_4$ NPs before pyrolysis to produce CNF aerogels decorated with $Fe/Fe_3O_4$ core-shell structures. To our best knowledge, the magnetic functionalization of CNF from BC for oil absorption/separation has not been reported before. Several characterization techniques have been employed to confirm the phase formation, distribution, properties of the magnetic core-shell nanoparticles in the CNF aerogels. Absorption tests for various kinds of organic solvents and oils showed a very fast absorption rate. The absorption capacity was relatively high compared to other biomass-derived carbon aerogels. The fabricated aerogels also possess unique characteristics, such as being ultralight weight, hydrophobic/oleophilic, highly compressible, recyclable, magnetic motionable and retractable.

## Results and discussion

The synthesis procedures as well as the absorption measurements are summarized in Scheme 1. The morphologies of the BC, CNF, magnetic BC (MBC), and magnetic CNF (MCF) aerogels are presented in Fig. 1. All aerogels consist of a 3D interconnected structure of nanofibers (diameters <100 nm) of very high porosity (> 99%). The surfaces of the MBC1 and MCF1 nanofibers (the suffix 1 is related to NP concentrations, as discussed later) are uniformly coated with $Fe_3O_4$ NPs. No obvious aggregation of the NPs is observed, suggesting that the fabrication method is appropriate in preparing highly dispersed NPs in BC and CNF aerogels. The characteristic functional groups of BC are present for the BC and MBC1 aerogels, but absent for the CNF and MCF1 aerogels (Fig. S1 in Supporting Information, SI). Instead, the main peaks of C-C, C=C and C≡C bonds are observed in the CNF aerogel, indicating the formation of a carbon structure. Similar functional groups are found in MCF1 but the peak intensities are much weaker.

Magnetic measurements show that magnetization is induced in both the MBC1 and MCF1 aerogels (Fig. 1e), but magnetic hysteresis is not observed, which would imply superparamagnetism, due to the nanosize of the NPs.[42-43] The inset of Fig. 1e shows a picture of the MCF1 aerogel which is being magnetically lifted by a magnet. Also, a drop of water is suspended on top of the aerogel surface, demonstrating its hydrophobic property. The saturation magnetization ($M_s$) increased from ~6 emu $g^{-1}$ for MBC1 to >100 emu $g^{-1}$ for MCF1. The $M_s$ of the MCF1 aerogel is much higher than the values reported for other magnetic oil sorbents: CNT (21.1 emu $g^{-1}$),[44] PU (13-40 emu $g^{-1}$),[7,45-46] cellulose (30-45 emu $g^{-1}$)[26-27,47] In fact, the present $M_s$ value is larger than that of bulk $Fe_3O_4$ (~92 emu $g^{-1}$).[48] The reasons for this exceptionally high $M_s$

value can be explained based on energy-dispersive X-ray spectroscopy (EDS) analysis (Fig. 1f) and transmission electron microscope (TEM) images (Fig. 2). The EDS spectrum shows exceptionally intense Fe peaks with respect to the O peak, in a carbon matrix (CNF). The larger proportion of Fe (19.6 at.%) compared to O (12.8 at.%) suggests that the NPs are in mixed phases between metallic Fe and Fe oxides. This interpretation is supported by TEM images (Fig. 2) which show the core-shell structure of the isolated NPs anchoring on the amorphous CNF. The core-shell structure is very obvious in the high-resolution image (Fig. 2b,c) and in the angle annular dark-field (HAADF) image (Fig. 2d), showing the bright contrast core and the fainter contrast shell. The EDS mapping of the particles reveals an enriched (depleted) region of Fe (O) in the centre and vice versa in the outer surface of the NPs (Fig. 2e-g).

To confirm the core-shell structure of the NPs in the MCF1 aerogel, further X-ray related techniques were utilized. Fig. 3a shows X-ray diffraction (XRD) patterns of the BC, CNF, MBC1 and MCF1 aerogels to determine their phase evolution. The BC aerogel shows characteristic peaks located at 14.0°, 16.5° and 22.3° corresponding to the $(1\bar{1}0)$, (110) and (200) diffraction planes, respectively,[49] while the CNF aerogel exhibit a broad hump at around 24°, a signature for amorphous carbon. The MBC1 aerogel exhibits additional peaks besides those characteristic of cellulose, which are attributed to $FeC_4H_2O_4$ (ICDD: 00-023-173) and $Fe_3O_4$, (ICDD: 01-089-0688). After pyrolysis, the MCF1 sample formed combined phases of amorphous carbon, metallic Fe, and $Fe_3O_4$; the major crystalline phase belongs to metallic Fe (ICDD: 01-087-0722). Furthermore, an X-ray absorption spectroscopy (XAS) study for the Fe K-edge energy was carried out. As shown in Fig. 3b, the XAS energy edge of the MCF1 sample lies in between the energy edges of the $Fe_3O_4$ and Fe references. This technique again confirms the formation of the mixed phases between Fe and $Fe_3O_4$. Finally, to verify the Fe core - $Fe_3O_4$ shell structure of the NPs, the MCF1 aerogel was subjected to X-ray photoelectron spectroscopy (XPS) analysis, which is a more surface-sensitive technique than XRD or XAS. The XPS analysis is thus focused on the 'shell' of the NPs. Fig. 3c shows a wide scan XPS spectrum which reveals the mixed composition of C, Fe and O. The high-resolution Fe2p spectrum shows the $Fe2p_{1/2}$ and $Fe2p_{3/2}$ peaks located at 724.5 eV and 710.9 eV, respectively, which correspond to the Fe2p peaks for $Fe_3O_4$.[50-51] Moreover, the O1s peak at the binding energy of 530.1 eV is ascribed to the oxygen in $Fe_3O_4$,[52] confirming the formation of the $Fe_3O_4$ shell structure.

The above analysis assures that the NPs in the MCF1 aerogel comprise a $Fe/Fe_3O_4$ core-shell structure. This is the reason for the very high $M_s$ of the MCF1 aerogels since the $M_s$ of the metallic Fe is 218 emu $g^{-1}$ at room temperature, much higher than that of $Fe_3O_4$.[48] The conversion of metal oxide NPs to metallic NPs in the presence of the BC matrix during pyrolysis has been reported in the literature.[35,41,53] The critical parameters for this to occur are the pyrolysis temperature and concentration of NPs. For example, Liu *et al.* fabricated CNF-supported $CoFe_2O_4$ NPs by pyrolysis of $BC/CoFe_2O_4$ nanocomposites at a relatively low temperature (500 °C).[35] The $CoFe_2O_4$ NPs remain in the same oxide phase in the CNF matrix after the pyrolysis process. On the other hand, metallic ions (Fe, Co, Ni), in the presence of BC nanofibers, have been converted to carbon-coated metallic NPs by pyrolysis at 800 °C in a $N_2$ atmosphere.[53] In addition, Wan *et al.* showed that by pyrolyzing the $BC/Fe_2O_3$ aerogel at 600 °C in $N_2$, the reduced atmosphere transforms the aerogel to a $CNF/Fe_3O_4$ composite.[41] Similarly, the conversion of iron oxides ($Fe_2O_3$ and $Fe_3O_4$) to metallic iron in the presence of cellulose has been observed in the pyrolysis temperature range of 600 – 800 °C.[54-55] This is analogous to a smelting process where iron is extracted from iron ore in the presence of carbon. In this case, the carbon source is the bacterial cellulose fibers. The reason that the $Fe/Fe_3O_4$ core-shell structure is found in the current work is perhaps because of the insufficiently high temperature and the lack of a pure carbon source, so that full conversion does not occur. This lack of a full conversion though does encapsulate the iron particles within a carbon shell, which enables consolidation of the structure. The pyrolysis conditions - 700 °C in an Ar atmosphere - is optimal to convert the MBC nanocomposite precursor to a CNF matrix decorated with highly dispersed $Fe/Fe_3O_4$ core-shell NPs.

It is also interesting to investigate the effect of the NP concentration on the structure, morphology and properties of the MBC and CNF aerogels. Thermogravimetric (TGA) analysis (Fig. S2 in SI) shows that the amount of the retained NPs in the MBC aerogels increased with increasing concentration of the iron ions in the co-precipitation process (from MBC1 to MBC4). However, increasing the number of NPs does not strongly affect the morphology of the MBC aerogels (Fig. S3 in SI); they still consist of 3D interconnecting carbon nanofibers with high porosity. The larger NP content only leads to a thicker coating of NPs on the surface of the BC nanofibers. Furthermore, the XRD analysis of the MBC aerogels (Fig. S4a in SI) shows the increasing intensity of the $Fe_3O_4$ peaks with respect to the BC peaks for increasing NP concentrations (MBC1 to MBC4), thus confirming the formation of the $Fe_3O_4$ magnetic phase in

BC aerogels. The results are well supplemented by the magnetic measurement for which the $M_s$ values increase as a function of NP concentration (Fig. S5a in SI).

A more noticeable change in the morphology of the nanofiber is found for the case of the MCF aerogels. This changes from highly dispersed NPs in the carbon fiber matrix for the low NP concentration (MCF1 and MCF2) to the clustered particles for the samples with higher concentration (MCF3, MCF4) (Fig. S6 (in SI)). In particular, for the highest NP concentration (MCF4), the uptake volume of NPs is exceedingly large so that the magnetic clusters merge into substantially larger particles (70.4 ± 26.9 nm). Also, the CNF matrix is so crowded by NPs that individual nanofibers cannot be visualized. Interestingly, the magnetic measurement of the MCF aerogels does not follow the same trend as for the MBC aerogels. (Fig. S5b in SI). The $M_s$ increases from 102 emu $g^{-1}$ for MCF1 to 172 emu $g^{-1}$ for MCF2 but decreases to 74 emu $g^{-1}$ and 85 emu $g^{-1}$ for MCF3 and MCF4, respectively. The variation of the magnetization can be explained from the phase formation of the MCF aerogels. For low NP concentration (MCF1 and MCF2), the XRD analysis shows the combined magnetic phases of $Fe_3O_4$ and metallic Fe while only the $Fe_3O_4$ magnetic phase is found for high NP concentration (MCF3 and MCF4) (Fig. S4b in SI). Since $M_s$ of Fe is much higher than that of $Fe_3O_4$,[48] it is justified for the larger $M_s$ values for MCF1&2 compared to those of MCF3&4. Another interesting point to conclude is that the concentration of NPs in the BC matrix can crucially affect the magnetic phases of the MCF aerogels. Only the right amount of NPs can yield the $Fe/Fe_3O_4$ core-shell structure in the CNF matrix whereas excessive NPs in BC lead to MCF aerogels with the combined phases of amorphous carbon and $Fe_3O_4$.

One big advantage of carbon aerogels is an ultralight weight property and an ultralow density ranging from a few mg $cm^{-3}$ to tens of mg $cm^{-3}$ depending on the carbon source and fabrication method.[4] In this work the CNF aerogel derived from BC is ultralight weight, with a density of only 3.2 ± 0.1 mg $cm^{-3}$, which is considered comparable or even lighter to the data for the biomass-based carbon aerogels in the literature; for instance, poplars catkins (4.3 mg $cm^{-3}$),[14] cellulose microfibrils (10 mg $cm^{-3}$),[56] cotton (12 mg $cm^{-3}$),[12] waste paper (5.8-23.6 mg $cm^{-3}$),[18-19,57] and winter melon (48 mg $cm^{-3}$).[13] In addition, the density of the CNF aerogel in the present work is also comparable to previously reported carbon aerogels from BC (4-6 mg $cm^{-3}$) that were carbonized at higher pyrolysis temperatures (up to 1300 °C).[17] The integration of magnetism in aerogels generally leads to a much heavier weight since magnetic components are more dense.[24] However, in this work, we successfully fabricated ultralight magnetic CNF aerogel (MCF1) with

a density of only 7.4 ± 1.2 mg $cm^{-3}$. This is comparable to or even lighter than other magnetic carbon aerogels from several carbon sources reported previously; namely, graphene oxide,[58] CNT,[44] cotton,[26] and popcorn,[15] which possess densities of 9, 15, 36, and 95 mg $cm^{-3}$, respectively. Moreover, the density of the MCF1 aerogel is comparable to the ultralow density (6-11 mg $cm^{-3}$) of the 3D magnetic iron oxide frameworks prepared by an interfacial assembly of Prussian Blue nanocubes,[59] and lower than magnetic melamine foams (13.9 mg $cm^{-3}$).[60] Fig. 4a (and Fig. S7 in SI) demonstrates the ultralight weight of the MCF1 aerogel which can be placed on top of a flower without deflecting it. Nevertheless, the density of the MCF aerogels increases significantly with an increasing NP content (Fig. S8 in SI). For example, the density of the MCF2 aerogel increases to 20.3 ± 1.0 mg $cm^{-3}$, equivalent to a >500% increase in the density compared to the pristine CNF aerogel.

To apply the MCF aerogels for selective oil absorption application, the hydrophobic property of the aerogel is of great importance. Fig. 4b shows the contact angle measurement of a drop of water on the surface of the aerogels. The contact angle is 98.6 ± 1.5 ° for the pristine CNF aerogel, and increases to 107.2 ± 3.5° and 131.0 ± 1.6° for MCF1 and MCF2, respectively. The contact angle of the CNF aerogel in this work is still much lower than that of the CNF aerogel reported previously (contact angles in the range 116.8-144°).[17,32,56] However, previous research employed higher pyrolysis temperatures (800-1300 °C),[17,32,56] resulting in a purer carbon structure and thus increased hydrophobicity. The increased contact angles for the MCF1 and MCF2 aerogels in Fig. 4b are attributed to the Wenzel wetting effect[61] from an increased surface roughness of the carbon nanofibrils due to the NPs anchoring on individual nanofibers. Also, the NPs are still covered with thin carbon layers; thus, the free surface energy is not altered. On the other hand, the MCF aerogels become hydrophilic when the higher NP concentrations are impregnated (MCF3 and MCF4). The possible explanation is that the amount of NPs in these samples is exceedingly large that they cover the whole surface of the nanofibers (Fig. S6 in SI), thus totally blocking the carbon fiber surfaces exposed to the water drop and increase the surface energy of the system.

For practical applications, mechanical performance is another important parameter for oil sorbents. CNF aerogels are well known for their outstanding mechanical properties, especially their flexibility and recovery to their original shape after compressive deformation.[17,19,33] However, it has been shown that the incorporation of NPs in BC aerogels resulted in the deterioration of mechanical properties since they cause interruption of the inter-fibril interactions.[42] In this work,

we demonstrate that the MCF aerogels still demonstrate excellent mechanical properties. Fig. 4c presents typical cyclic compressive stress-strain curves of the MCF1 aerogels with different maximum strains (50-90%). Hysteresis loops appear in the loading-unloading cycles, indicating the dissipation of mechanical energy due to friction between flowing air and the CNF skeleton.[62] Three distinct stages during the compressive process are observed, namely, an initial linear region, a gradually increasing slope, and finally a quick increase in the stress, as observed in other carbon aerogels.[17,32] In the unloading process, the stress remains above zero, and returns to the initial point, indicating complete elastic recovery without plastic deformation. The photographs of the MCF1 aerogel during the compression test at a maximum strain of 90% show good recovery under large compressive deformation (Fig. 4e). Furthermore, the MCF1 aerogel was subjected to a cyclic compression test with 100 loading-unloading cycles at a maximum strain of 50% to evaluate the durability of the aerogel. The MCF1 aerogel can withstand 100 successive cycles and still retains its original shape without fracture or collapse (Fig. 4d). In addition, Fig. 4f shows the hand squeezing of the MCF1 aerogel from the sides for which the aerogel instantly restores to its original shape. The compressive test results suggest that the MCF1 aerogels show excellent mechanical compressibility, which is rare for carbon aerogels prepared from cellulose,[19] and robust mechanical performance comparable or even better than some pristine carbon aerogels.[14,63-64] This robustness could be attributed to the highly dispersed NPs in the 3D CNF network structure for which the NPs do not interrupt the inter-fibril interactions, and thus preserve the outstanding mechanical properties.

Owing to its ultralow density, high porosity, hydrophobic property and outstanding mechanical properties, as well as ferromagnetic functionality, the MCF1 aerogel is an ideal candidate for the absorption and recycling of oils and organic solvents from wastewater. As shown in Fig. 5a, a piece of the MCF1 aerogel is placed in a container filled with gasoline. Within a few seconds, it completely absorbs the gasoline with a high absorption capacity (>65 times of the aerogel's weight). Moreover, it can be easily retrieved by magnetic extraction after absorption takes place. Due to its ultralight weight, the MCF1 aerogel can be used to absorb oils floating on the water surface (Fig. 5b). An external magnetic field can be applied to control the motion of the aerogel in the liquid. This functionality is very useful for manipulating the sorbents in a large area of polluted water. After the oil is completely absorbed, the aerogel is easily removed from the water by the same magnetic field. The MCF1 aerogels were tested as sorbents for various kinds of

oils and organic solvents, which are common pollutants in daily life or industry. As presented in Fig. 5c, the mass absorption capacities of MCF1 are in the range of 37-87 g/g. (The volume absorption capacity is shown in Fig. S9 in SI.) These values are still much lower than some previous reports for the pristine CNF aerogels from several sources, such as CNT (80-180 g/g),[10] graphene (200-600 g/g),[11] graphene-CNT (215-913),[64] BC (106-312 g/g),[17] BC-graphene (243-457 g/g),[32] and BC-graphene oxide (393-1002 g/g).[33] However, they are comparable or even better than other pristine carbon aerogels from various sources, for example, CNF sponge (22-75),[63] cotton (22-87),[26] winter melon (16-50 g/g),[13] popcorn,[15] bamboo (23-51 g/g),[16] wastepaper (29-51 g/g),[57] cellulose microfibrils (48-87 g/g),[56] and BC/polyimide (10-40 g/g).[31] The reasons for these large absorption capacities is due to the uniformly and loosely distributed NPs in the CNF structure (Figs. 1 and 2) for which the carbonaceous surface of the fibers and the high porosity of the aerogel are preserved, resulting in hydrophobic/oleophilic properties and large free space volume for oil uptake.

Generally, the magnetism integration and oil absorption performance show a trade-off effect.[60] In other words, the magnetic functionalization of a sorbent material often causes a reduction in oil absorption capacity. In the present work, the pristine CNF aerogels show superior absorption capacity compared to the MCF aerogels. For the absorption of gasoline, the CNF aerogel shows a very high absorption capacity of ~170 g/g, while the value significantly drops to ~67 g/g and ~27 g/g for MCF1 and MCF2, respectively (Fig. S10 in SI). Although higher water contact angles are observed for MCF1 and MCF2 with respect to the CNF aerogel (Fig. 4b), which indicates enhanced hydrophobic/oleophilic properties; the incorporation of NPs increases the sorbent density (Fig. S8 in SI), and thus reduces the absorption capacity.[65]

Nevertheless, the absorption capacity of oils/organic solvents for the MCF1 aerogel is still very high compared to other magnetic carbon aerogels reported in the literature. Table 1 compares the absorption capacities of magnetic carbon aerogels from various sources, including the present work. As for an explicit comparison, the absorption capacities of toluene for various sorbents are also presented. Table 1 summarizes the fabrication methods, magnetic materials, surface modifiers, water contact angle, density, and saturation magnetization ($M_s$) of the magnetic carbon sorbents. Compared with the literature, the advantages of the MCF1 aerogel in the present work are the utilization of the biomass carbon source which is cheap and abundant, the ease of fabrication method, and the lack of a need for further surface treatments. The absorption capacity

is of the same order or superior to most sorbents. Moreover, though the MCF1 aerogel possesses an ultralow density, it exhibits a very high $M_s$ value, due to the presence of the $Fe/Fe_3O_4$ core-shell nanostructure. The large magnetization of the aerogel sorbent is very useful. For bare aerogels, the magnetization values may not be very important for magnetic lifting or movement controlling since the aerogel itself is very light. The $M_s$ values of only a few emu $g^{-1}$ are more than sufficient for magnetic attraction. However, after the absorption of oils/organic solvents, the aerogels can be up to tens or even hundreds of times heavier than their original states. These heavier weights will cause a problem for magnetic manipulation of the sorbents with low magnetization values.

Recovery and reusability of the aerogel after oil absorption is very important. Recovery can be carried out by magnetic retraction of the MCF aerogel owing to its ferromagnetic property. This functionality is advantageous since direct contact with toxic or harmful solvents can be avoided. For reusability, due to the robustness and large compressibility of the MCF1 aerogel (Fig. 4e), the aerogels can be squeezed to extract the oils. However, the squeezing method is not chosen since not all liquid can be squeezed out, and also to avoid direct contact with the solvents. Instead, the dissolution method is used. The oil-absorbed aerogel is washed with hexane before drying at 80 °C. Since hexane has a low boiling point (68 °C), it is easily evaporated from the MCF aerogel. The recycling experimental result of gasoline absorption is shown in Fig. 5d. After 5 cycles, a reduction in the absorption capacity of ~29% is observed. It indicates that though the MCF1 aerogel can be reused several times, the absorption capacity is gradually reduced over time. The reasons for the reduction in absorption capacity is possibly due to a slight change in surface functional groups and the morphology of the CNF. The FTIR spectra of the MCF1 before and after oil absorption are shown in Fig. 5e. The absorbed aerogel shows the same characteristic functional groups as for the gasoline. After oil removal, the functional groups are almost absent, and the MCF1 shows the FTIR spectra nearly the same as before oil absorption. The surface morphology of the MCF1 aerogel after oil desorption is shown in Fig. 5f. It clearly shows that the 3D structure network of the CNF with highly dispersed NPs is still preserved. The TGA measurement of the samples after oil absorption (not shown) has verified that the amount of the NPs in the MCF1 aerogel remained the same. However, the pore structure may be slightly changed as compared to the original aerogel before absorption (Fig. 1d).

In addition, the MCF1 aerogel was demonstrated for the absorption of the submerged oil under water, as shown in Fig. 6a. When the MCF1 aerogel was immersed into water, air bubbles

entrapped at the interface between the aerogel and the surrounding water were clearly observed. And once the aerogel was in contact with the submerged oil (dichloromethane), it instantly absorbed the oil droplet completely. Furthermore, the this MCF1 sample can be applied as a membrane for oil/water separation. As demonstrated in Fig. 6b, when the oil/water mixture was poured in the upper part of the tube, the MCF1 aerogel only allows oil (dichloromethane) to pass through whereas water cannot penetrate. The separation efficiency was found to be as high as 98%. This experiment demonstrated that though the contact angle of the MCF1 aerogel is relatively lower than other previous reports, it can still be effectively used as an oil/water separation membrane. Due to this ability, we believe that the MCF1 aerogel can be further applied for the separation of emulsions.

## Conclusions

In summary, by varying NP concentrations and using a relatively low pyrolysis temperature, we have successfully fabricated uniformly dispersed magnetic core-shell nanoparticles in carbon nanofiber aerogels derived from magnetic BC nanocomposites. The MCF aerogels consisting of Fe core/$Fe_3O_4$ shell NPs coated by a thin carbon layer exhibit several unique and outstanding properties. The saturation magnetization ($M_s$) is very high (~102 emu $g^{-1}$), compared to other magnetic aerogels previously studied, due to the presence of the Fe/$Fe_3O_4$ core-shell structure. Despite the high $M_s$, the MCF aerogel is still very light with a density of only 7.4 ± 1.2 mg $cm^{-3}$. Without any post-surface treatment, the MCF aerogel shows hydrophobic/oleophilic properties with a water contact angle of ~107° Besides this, it also possesses excellent mechanical properties. The compressibility can be as high as 90% strain and it can be restored to the original shape instantly without deformation. It is also durable for 100 compressive stress-strain cycles without any change in shape. Moreover, the MCF aerogel is an ideal candidate as a sorbent for oils and organic solvents. Although the integration of magnetism in the CNF aerogel leads to a reduction in oil absorption capacity, the MCF aerogel still shows a relatively large absorption capacity (37-87 g/g) for a wide range of oils/solvents. The large magnetization makes it easy to be manipulated or retrieved after absorption which is advantageous for avoiding direct contact with possible toxic solvents. The MCF aerogel can be recycled several times with only a slight drop in absorption capacity. The present work demonstrates an exciting prospect for using these materials to alleviate oil spills and pollution incidents, which will have huge positive benefits to the environment.

**Table 1.** Comparison of various types of magnetic carbon aerogels for oil sorption.

| Sorbents | Carbon source, (method) | Magnetic materials, (surface modifier) | contact angle (°) | Sorbent density (mg $cm^{-3}$) | $M_s$ (emu $g^{-1}$) | Sorption capacity (g/g) (toluene) | Ref. |
|---|---|---|---|---|---|---|---|
| Magnetic foam | PU (pyrolysis) | $Fe_2O_3$, (MTS) | 152 | 3.9 | 17.2 | 61.8-102.6 (n/a) | [7] |
| Magnetic porous carbon aerogel | Popcorn (pyrolysis) | Fe oxides, (OCS) | 151.6 | 95 | 3.3 | ~10 (n/a) | [15] |
| Magnetic PDMS/MWNT nanocomposites | MWNT, (mixing, infiltrating, curing) | Commercial magnetic MWNT, (PDMS) | 153.4 | 308 | - | 8.8-20.5 (~12.5) | [25] |
| MCF aerogel | Cotton, (pyrolysis) | $Fe_3O_4$, (n-hexane) | >140 | - | 23.9 | 29-70 (29) | [27] |
| CNT sponge | CNT, (CVD) | Encapsulated Fe | >140 | 15 | 21.1 | ~66 (n/a) | [44] |
| Cobalt-doped carbon aerogel | Graphene oxide, (chemical synthesis, purification, pyrolysis) | $Co/C_xO_y$ | - | 9 | 18 | 47-132 (~58) | [58] |
| MCF aerogel | Na CMC/Na MMT, (pyrolysis) | Fe oxides | 121 | 64 | 31.1 | 10-19 (n/a) | [66] |
| Magnetic porous MWNT beads | MWNT, (microfluidic, thermal treatment) | $Fe_3O_4$ | 152 | - | - | 6-18 (~12) | [67] |
| MCF aerogel | BC, (pyrolysis) | $Fe/Fe_3O_4$ core-shell | 107.2 | 7.4 | 102 | 37-89 (89) | this work |

MTS – methyltrichlorosilane, OCS – octyltrichlorosilane, MWNT – multiwalled carbon nanotube, PE – polyethelene, PFOS – perfluorooctyltriethoxysilane,

## Experimental section

### Production of bacterial cellulose

Bacterial cellulose (BC) pellicle was prepared from the biosynthesis of the bacterial strain *Gluconacetobacter xylinum* (strain TISTR 975), supplied from the Microbiological Resources Centre, Thailand Institute of Scientific and Technological Research (TISTR). A single colony of bacteria was transferred into 50 mL of a liquid culture medium, which consists of 100 g of anhydrous D-glucose (Ajax Finechem) and 10 g of yeast extract powder (HiMedia) in 1 L of distilled water. After 24 h of cultivation at 30 °C in a shaker incubator (150 rpm), 1 mL of the cell suspension was introduced into a container containing 50 mL of a fresh liquid culture medium and then cultivated at 30 °C for 14 days under static conditions. The obtained BC pellicle was purified by boiling in distilled water for 1 h. This boiling step was repeated twice. The BC pellicle was then purified with 0.5 M sodium hydroxide solution for 15 min, followed by soaking in 5% sodium hydroxide solution for 24 h at room temperature. Finally, it was washed in distilled water until the BC pellicle became neutral. The purified BC was freeze-dried and kept at room temperature prior to use.

### Preparation of BC/$Fe_3O_4$ nanocomposites

The iron chloride solution was prepared by mixing ferric chloride ($FeCl_3 \cdot 6H_2O$) (QRëC, analytical grade) and ferrous chloride ($FeCl_2 \cdot 4H_2O$) (Merck, analytical grade), using the molar ratio of 2:1. The freeze-dried BC was immersed in 200 mL of the prepared solution for 20 min at room temperature. The color of the BC gradually changed from white to yellow. Then, the solution containing the BC was heated to 50 °C and held for 1 h. After that, the BC pellicle was transferred to a 1.2 M sodium hydroxide solution (RCI Labscan, analytical grade) and kept at 50 °C for 30 min. The color of the BC changed rapidly from yellow to black, indicating the formation of the NP phases. The obtained product was then washed with distilled water until neutral. The hydrogel was freeze-dried to obtain the magnetic BC (MBC) aerogel. To study the effect of NP concentration, concentrations of $FeCl_3 \cdot 6H_2O$ of 12.5, 25, 50 and 100 mM were used which corresponded to the samples MBC1, MBC2, MBC3 and MBC4, respectively.

**Preparation of magnetic carbon nanofiber (MCF)**

The MBC nanocomposites were transferred into a tubular furnace for pyrolysis under an argon atmosphere. The samples were heated to 500 °C at a heating rate of 2 °C $min^{-1}$ and kept at this temperature for 1 h. Then they were heated to 700 °C using a rate of 5 °C $min^{-1}$, and held at this temperature for 2 h to allow complete carbonization of BC. Finally, it was cooled to room temperature naturally. After the process, ultralight weight magnetic carbon nanofiber (MCF) aerogels were obtained. The magnetic aerogels with different NP concentrations are denoted as MCF1, MCF2, MCF3 and MCF4, and the pristine carbon nanofiber aerogel is referred to as CNF.

**Characterization**

The surface morphology and the distribution of NPs in the MBC and MCF aerogels were observed by using a field emission scanning electron microscope (FE-SEM) (FEI, Helios, USA). Prior to imaging, the samples were gold coated to improve conductivity. The size and morphology of NPs distributed in the CNF aerogels were observed using a field emission transmission electron microscope (FE-TEM) (Thermo Scientific, TALOS F200X, USA). The chemical compositions of the samples were verified by using energy-dispersive X-ray spectroscopy (EDS) equipped with the FE-SEM and FE-TEM. The functional groups of the samples were investigated using Fourier transform infrared (FTIR) spectroscopy (Bruker, TENSOR27, Germany). The magnetic property measurement was carried out using a vibrating sample magnetometer (VSM) option in the VersaLab instrument (Quantum Design, USA). The thermal analysis of the MBC aerogels was studied using a thermogravimetric analysis (TGA) technique (Hitachi, STA7200, Japan). Information on the crystalline structures of the samples was collected by using X-ray diffraction (XRD) with a diffractometer employing Cu-Kα radiation (PANalytical, Empyrean, USA). The bulk density ($\rho$) was calculated from the mass and volume measurements. The porosity ($P$) was calculated from the equation: $P(\%) = (1 - \rho/\rho_m) \times 100$,[56] where $\rho_m$ is the skeletal density of CNF and NP, estimated from the weighted average density. The water contact angle (WCA) on the surface of the aerogels was measured with a specialized instrument (FTA1000 Drop Shape Analysis System, UK). Compressive stress-strain curves were measured using a universal testing machine (UTM, Instron 5567A, USA). In addition, X-ray absorption spectroscopy (XAS) of Fe K-edge was conducted at the Time-resolved X-ray Absorption Spectroscopy (TRXAS) at beamline (BL2.2), and the surface composition of the MCF sample were measured using X-ray

photoelectron spectroscopy (XPS, PHI5000 VersaProbe II, ULVAC-PHI), at the SUT-NANOTEC- SLRI research facility, Synchrotron Light Research Institute (SLRI), Thailand.

**Absorption measurement**

In a typical measurement, the MCF aerogel was weighed before immersing into various kinds of oils/organic solvents for 10 min, and then it was taken out for weight measurement again. The absorption capacity ($q$) is defined $q = (m_f - m_i)/m_i$, where $m_i$ and $m_f$ are the masses of the MCF aerogel before and after oil/solvent absorption. All absorption experiments were repeated 5 times to obtain average absorption capacities. For the recyclability of the MCF aerogels, after oil absorption, the sorbents were washed with hexane thoroughly before oven-drying at 80 °C. The weight after drying was carefully measured before repeating the absorption experiment. For oil/water separation, the separation efficiency ($S_e$) was determined by the equation: $S_e = m_{w1}/m_{w0} \times 100$ , where $m_{w0}$ and $m_{w1}$ are the masses of water before and after separation, respectively.

## Supporting Information

Additional information on several characterization techniques: FTIR, TGA, SEM, XRD, VSM, and TEM. Density measurement and lightweight demonstration. More information on mass absorption capacity and volume absorption capacity.

## Conflicts of Interest

There are no conflicts of interest to declare.

## Acknowledgments

This work was supported by the Thailand Research Fund (TRF) in cooperation with Synchrotron Light Research Institute (public organization) and Khon Kaen University (RSA6280020), the Royal Society-Newton Advanced Fellowship (NA160147) in partnership with the Thailand Research Fund (TRF) (DBG6080002), the Royal Golden Jubilee Ph.D. Programme (PHD/0052/2560), and the Research Network NANOTEC (RNN) program of the National Nanotechnology Center (NANOTEC), NSTDA, Ministry of Higher Education, Science, Research and Innovation, and Khon Kaen University, Thailand.

## References


1. Schrope, M., Oil Spill Deep Wounds. *Nature* **2011,** *472*, 152-154.
2. Jeddi, M. K.; Laitinen, O.; Liimatainen, H., Magnetic Superabsorbents Based on Nanocellulose Aerobeads for Selective Removal of Oils and Organic Solvents. *Mater. Design* **2019,** *183*, 108115.
3. Ge, J.; Zhao, H. Y.; Zhu, H. W.; Huang, J.; Shi, L. A.; Yu, S. H., Advanced Sorbents for Oil-Spill Cleanup: Recent Advances and Future Perspectives. *Adv. Mater.* **2016,** *28*, 10459-10490.
4. Chen, B.; Ma, Q. L.; Tan, C. L.; Lim, T. T.; Huang, L.; Zhang, H., Carbon-Based Sorbents with Three-Dimensional Architectures for Water Remediation. *Small* **2015,** *11*, 3319-3336.
5. Gupta, S.; Tai, N. H., Carbon Materials as Oil Sorbents: A Review on the Synthesis and Performance. *J. Mater. Chem. A* **2016,** *4*, 1550-1565.
6. Du, R.; Gao, X.; Feng, Q. L.; Zhao, Q. C.; Li, P.; Deng, S. B.; Shi, L. R.; Zhang, J., Microscopic Dimensions Engineering: Stepwise Manipulation of the Surface Wettability on 3d Substrates for Oil/Water Separation. *Adv. Mater.* **2016,** *28*, 936-942.
7. Chen, N.; Pan, Q. M., Versatile Fabrication of Ultralight Magnetic Foams and Application for Oil-Water Separation. *ACS Nano* **2013,** *7*, 6875-6883.
8. Wang, X. F.; Yu, J. Y.; Sun, G.; Ding, B., Electrospun Nanofibrous Materials: A Versatile Medium for Effective Oil/Water Separation. *Mater. Today* **2016,** *19*, 403-414.
9. Deuber, F.; Mousavi, S.; Federer, L.; Adlhart, C., Amphiphilic Nanofiber-Based Aerogels for Selective Liquid Absorption from Electrospun Biopolymers. *Adv. Mater. Interfaces* **2017,** *4*, 1700065.
10. Gui, X. C.; Wei, J. Q.; Wang, K. L.; Cao, A. Y.; Zhu, H. W.; Jia, Y.; Shu, Q. K.; Wu, D. H., Carbon Nanotube Sponges. *Adv. Mater.* **2010,** *22*, 617-621.
11. Zhao, Y.; Hu, C. G.; Hu, Y.; Cheng, H. H.; Shi, G. Q.; Qu, L. T., A Versatile, Ultralight, Nitrogen-Doped Graphene Framework. *Angew. Chem. Int. Edit.* **2012,** *51*, 11371-11375.
12. Bi, H. C.; Yin, Z. Y.; Cao, X. H.; Xie, X.; Tan, C. L.; Huang, X.; Chen, B.; Chen, F. T.; Yang, Q. L.; Bu, X. Y.; Lu, X. H.; Sun, L. T.; Zhang, H., Carbon Fiber Aerogel Made from Raw Cotton: A Novel, Efficient and Recyclable Sorbent for Oils and Organic Solvents. *Adv. Mater.* **2013,** *25*, 5916-5921.
13. Li, Y. Q.; Samad, Y. A.; Polychronopoulou, K.; Alhassan, S. M.; Liao, K., Carbon Aerogel from Winter Melon for Highly Efficient and Recyclable Oils and Organic Solvents Absorption. *ACS Sustain. Chem. Eng.* **2014,** *2*, 1492-1497.
14. Li, L. X.; Hu, T.; Sun, H. X.; Zhang, J. P.; Wang, A. Q., Pressure-Sensitive and Conductive Carbon Aerogels from Poplars Catkins for Selective Oil Absorption and Oil/Water Separation. *ACS Appl. Mater. Inter.* **2017,** *9*, 18001-18007.
15. Dai, J. D.; Zhang, R. L.; Ge, W. N.; Xie, A. T.; Chang, Z. S.; Tian, S. J.; Zhou, Z. P.; Yan, Y. S., 3d Macroscopic Superhydrophobic Magnetic Porous Carbon Aerogel Converted from Biorenewable Popcorn for Selective Oil-Water Separation. *Mater. Design* **2018,** *139*, 122-131.
16. Jiao, Y.; Wan, C. C.; Li, J., Synthesis of Carbon Fiber Aerogel from Natural Bamboo Fiber and Its Application as a Green High-Efficiency and Recyclable Adsorbent. *Mater. Design* **2016,** *107*, 26-32.
17. Wu, Z. Y.; Li, C.; Liang, H. W.; Chen, J. F.; Yu, S. H., Ultralight, Flexible, and Fire-Resistant Carbon Nanofiber Aerogels from Bacterial Cellulose. *Angew. Chem. Int. Edit.* **2013,** *52*, 2925-2929.

18. Bi, H. C.; Huang, X.; Wu, X.; Cao, X. H.; Tan, C. L.; Yin, Z. Y.; Lu, X. H.; Sun, L. T.; Zhang, H., Carbon Microbelt Aerogel Prepared by Waste Paper: An Efficient and Recyclable Sorbent for Oils and Organic Solvents. *Small* **2014,** *10*, 3544-3550.
19. Li, L. X.; Li, B. C.; Sun, H. X.; Zhang, J. P., Compressible and Conductive Carbon Aerogels from Waste Paper with Exceptional Performance for Oil/Water Separation. *J. Mater. Chem. A* **2017,** *5*, 14858-14864.
20. Nagappan, S.; Ha, C. S., Emerging Trends in Superhydrophobic Surface Based Magnetic Materials: Fabrications and Their Potential Applications. *J. Mater. Chem. A* **2015,** *3*, 3224-3251.
21. Zhu, Q.; Tao, F.; Pan, Q. M., Fast and Selective Removal of Oils from Water Surface Via Highly Hydrophobic Core-Shell Fe2o3@C Nanoparticles under Magnetic Field. *ACS Appl. Mater. Inter.* **2010,** *2*, 3141-3146.
22. Flores, J. A.; Pavia-Sanders, A.; Chen, Y. C.; Pochan, D. J.; Wooley, K. L., Recyclable Hybrid Inorganic/Organic Magnetically Active Networks for the Sequestration of Crude Oil from Aqueous Environments. *Chem. Mater.* **2015,** *27*, 3775-3782.
23. Duan, C. T.; Zhu, T.; Guo, J.; Wang, Z.; Liu, X. F.; Wang, H.; Xu, X.; Jin, Y.; Zhao, N.; Xu, J., Smart Enrichment and Facile Separation of Oil from Emulsions and Mixtures by Superhydrophobic/Superoleophilic Particles. *ACS Appl. Mater. Inter.* **2015,** *7*, 10475-10481.
24. Du, R.; Zhao, Q. C.; Zheng, Z.; Hu, W. P.; Zhang, J., 3d Self-Supporting Porous Magnetic Assemblies for Water Remediation and Beyond. *Adv. Energy Mater.* **2016,** *6*, 1600473.
25. Turco, A.; Malitesta, C.; Barillaro, G.; Greco, A.; Maffezzoli, A.; Mazzotta, E., A Magnetic and Highly Reusable Macroporous Superhydrophobic/Superoleophilic Pdms/Mwnt Nanocomposite for Oil Sorption from Water. *J. Mater. Chem. A* **2015,** *3*, 17685-17696.
26. Liu, R. L.; Li, X. Q.; Liu, H. Q.; Luo, Z. M.; Ma, J.; Zhang, Z. Q.; Fu, Q., Eco-Friendly Fabrication of Sponge-Like Magnetically Carbonaceous Fiber Aerogel for High-Efficiency Oil-Water Separation. *RSC Adv.* **2016,** *6*, 30301-30310.
27. Li, Y.; Zhu, X. T.; Ge, B.; Men, X. H.; Li, P. L.; Zhang, Z. Z., Versatile Fabrication of Magnetic Carbon Fiber Aerogel Applied for Bidirectional Oil-Water Separation. *Appl. Phys. A-Mater.* **2015,** *120*, 949-957.
28. Huang, Y.; Zhu, C. L.; Yang, J. Z.; Nie, Y.; Chen, C. T.; Sun, D. P., Recent Advances in Bacterial Cellulose. *Cellulose* **2014,** *21*, 1-30.
29. Sai, H. Z.; Fu, R.; Xing, L.; Xiang, J. H.; Li, Z. Y.; Li, F.; Zhang, T., Surface Modification of Bacterial Cellulose Aerogels' Web-Like Skeleton for Oil/Water Separation. *ACS Appl. Mater. Inter.* **2015,** *7*, 7373-7381.
30. Wang, Y. G.; Yadav, S.; Heinlein, T.; Konjik, V.; Breitzke, H.; Buntkowsky, G.; Schneider, J. J.; Zhang, K., Ultra-Light Nanocomposite Aerogels of Bacterial Cellulose and Reduced Graphene Oxide for Specific Absorption and Separation of Organic Liquids. *RSC Adv.* **2014,** *4*, 21553-21558.
31. Lai, F. L.; Miao, Y. E.; Zuo, L. Z.; Zhang, Y. F.; Liu, T. X., Carbon Aerogels Derived from Bacterial Cellulose/Polyimide Composites as Versatile Adsorbents and Supercapacitor Electrodes. *Chemnanomat* **2016,** *2*, 212-219.
32. Wan, Y. Z.; Zhang, F. S.; Li, C. Z.; Xiong, G. Y.; Zhu, Y.; Luo, H. L., Facile and Scalable Production of Three-Dimensional Spherical Carbonized Bacterial Cellulose/Graphene Nanocomposites with a Honeycomb-Like Surface Pattern as Potential Superior Absorbents. *J. Mater. Chem. A* **2015,** *3*, 24389-24396.
33. Li, C.; Wu, Z. Y.; Liang, H. W.; Chen, J. F.; Yu, S. H., Ultralight Multifunctional Carbon-Based Aerogels by Combining Graphene Oxide and Bacterial Cellulose. *Small* **2017,** *13*, 1700453.

34. Cao, G. L.; Yan, Y. M.; Liu, T.; Rooney, D.; Guo, Y. F.; Sun, K. N., Three-Dimensional Porous Carbon Nanofiber Networks Decorated with Cobalt-Based Nanoparticles: A Robust Electrocatalyst for Efficient Water Oxidation. *Carbon* **2015,** *94*, 680-686.
35. Liu, S. S.; Yan, W. N.; Cao, X. C.; Zhou, Z. F.; Yang, R. Z., Bacterial-Cellulose-Derived Carbon Nanofiber-Supported Cofe2o4 as Efficient Electrocatalyst for Oxygen Reduction and Evolution Reactions. *Int. J. Hydrogen Energ.* **2016,** *41*, 5351-5360.
36. Huang, X. H.; Dai, B.; Ren, Y.; Xu, J.; Zhu, P., Preparation and Study of Electromagnetic Interference Shielding Materials Comprised of Ni-Co Coated on Web-Like Biocarbon Nanofibers Via Electroless Deposition. *J. Nanomater.* **2015**, 320306.
37. Huang, Y.; Lin, Z. X.; Zheng, M. B.; Wang, T. H.; Yang, J. Z.; Yuan, F. S.; Lu, X. Y.; Liu, L.; Sun, D. P., Amorphous Fe2o3 Nanoshells Coated on Carbonized Bacterial Cellulose Nanofibers as a Flexible Anode for High-Performance Lithium Ion Batteries. *J. Power Sources* **2016,** *307*, 649-656.
38. Liu, Z.; Wan, Y. Z.; Xiong, G. Y.; Guo, R. S.; Luo, H. L., Three-Dimensional Porous Nanocomposite of Highly Dispersed Fe3o4 Nanoparticles on Carbon Nanofibers for High-Performance Microwave Absorbents. *Mater. Express* **2015,** *5*, 113-120.
39. Luo, H. L.; Zhang, Y.; Yang, Z. W.; Xiong, G. Y.; Wan, Y. Z., Constructing Superior Carbon-Nanofiber-Based Composite Microwave Absorbers by Engineering Dispersion and Loading of Fe3o4 Nanoparticles on Three-Dimensional Carbon Nanofibers Derived from Bacterial Cellulose. *Mater. Chem. Phys.* **2017,** *201*, 130-138.
40. Ren, Y.; Dai, B.; Wang, G. H.; Zhang, X. W.; Zhu, P.; Li, S. R., Preparation and Microwave Absorption Properties of Novel Carbon Nanofiber/Fe3o4 Composites. *J. Nanosci. Nanotechno.* **2015,** *15*, 2845-2849.
41. Wan, Y. Z.; Yang, Z. W.; Xiong, G. Y.; Guo, R. S.; Liu, Z.; Luo, H. L., Anchoring Fe3o4 Nanoparticles on Three-Dimensional Carbon Nanofibers toward Flexible High-Performance Anodes for Lithium-Ion Batteries. *J. Power Sources* **2015,** *294*, 414-419.
42. Sriplai, N.; Mongkolthanaruk, W.; Eichhorn, S. J.; Pinitsoontorn, S., Magnetically Responsive and Flexible Bacterial Cellulose Membranes. *Carbohyd. Polym.* **2018,** *192*, 251-262.
43. Sriplai, N.; Koowattanasuchat, S.; Kidkhunthod, P.; Chanlek, N.; Eichhorn, S. J.; Pinitsoontorn, S., Magnetic Behavior of Novel Alloyed L1(0)-Phase Co1-Xfexpt Nanoparticles. *J. Alloy Compd.* **2018,** *739*, 19-29.
44. Gui, X. C.; Zeng, Z. P.; Lin, Z. Q.; Gan, Q. M.; Xiang, R.; Zhu, Y.; Cao, A. Y.; Tang, Z. K., Magnetic and Highly Recyclable Macroporous Carbon Nanotubes for Spilled Oil Sorption and Separation. *ACS Appl. Mater. Inter.* **2013,** *5*, 5845-5850.
45. Beshkar, F.; Khojasteh, H.; Salavati-Niasari, M., Recyclable Magnetic Superhydrophobic Straw Soot Sponge for Highly Efficient Oil/Water Separation. *J. Colloid Interf. Sci.* **2017,** *497*, 57-65.
46. Ge, B.; Zhu, X. T.; Li, Y.; Men, X. H.; Li, P. L.; Zhang, Z. Z., Versatile Fabrication of Magnetic Superhydrophobic Foams and Application for Oil-Water Separation. *Colloid Surface A* **2015,** *482*, 687-692.
47. Wang, H. W.; Chen, Y. P.; Dang, B. K.; Shen, X. P.; Jin, C. D.; Sun, Q. F.; Pei, J. C., Ultrafine Mn Ferrite by Anchoring in a Cellulose Framework for Efficient Toxic Ions Capture and Fast Water/Oil Separation. *Carbohyd. Polym.* **2018,** *196*, 117-125.
48. Cullity, B. D.; Graham, C. D., *Introduction to Magnetic Materials*. 2nd ed.; IEEE/Wiley: Hoboken, N.J., 2009; p xvii, 544 p.

49. Czaja, W.; Romanovicz, D.; Brown, R. M., Structural Investigations of Microbial Cellulose Produced in Stationary and Agitated Culture. *Cellulose* **2004,** *11*, 403-411.
50. Zhang, W. J.; Li, X. J.; Zou, R. T.; Wu, H. Z.; Shi, H. Y.; Yu, S. S.; Liu, Y., Multifunctional Glucose Biosensors from Fe3o4 Nanoparticles Modified Chitosan/Graphene Nanocomposites. *Sci. Rep.* **2015,** *5*, 11129.
51. Goncalves, L. C.; Seabra, A. B.; Pelegrino, M. T.; de Araujo, D. R.; Bernardes, J. S.; Haddad, P. S., Superparamagnetic Iron Oxide Nanoparticles Dispersed in Pluronic F127 Hydrogel: Potential Uses in Topical Applications. *RSC Adv.* **2017,** *7*, 14496-14503.
52. Ji, L. Q.; Zhou, L. C.; Bai, X.; Shao, Y. M.; Zhao, G. H.; Qu, Y. Z.; Wang, C.; Li, Y. F., Facile Synthesis of Multiwall Carbon Nanotubes/Iron Oxides for Removal of Tetrabromobisphenol a and Pb(Ii). *J. Mater. Chem* **2012,** *22*, 15853-15862.
53. Ma, B.; Huang, Y.; Zhu, C. L.; Chen, C. T.; Fan, M. M.; Sun, D. P., A Facile Method to Synthesize Carbon Coated Fe, Co and Ni and an Examination of Their Magnetic Properties. *J. Alloy Compd.* **2016,** *687*, 741-745.
54. Li, M.; Liu, H.; Chen, T.; Chen, D.; Wang, C.; Wei, L.; Wang, L., Efficient U(Vi) Adsorption on Iron/Carbon Composites Derived from the Coupling of Cellulose with Iron Oxides: Performance and Mechanism. *Sci. Total Environ.* **2020,** *703*, 135604.
55. Lotz, K.; Wutscher, A.; Dudder, H.; Berger, C. M.; Russo, C.; Mukherjee, K.; Schwaab, G.; Havenith, M.; Muhler, M., Tuning the Properties of Iron-Doped Porous Graphitic Carbon Synthesized by Hydrothermal Carbonization of Cellulose and Subsequent Pyrolysis. *ACS Omega* **2019,** *4*, 4448-4460.
56. Meng, Y. J.; Young, T. M.; Liu, P. Z.; Contescu, C. I.; Huang, B.; Wang, S. Q., Ultralight Carbon Aerogel from Nanocellulose as a Highly Selective Oil Absorption Material. *Cellulose* **2015,** *22*, 435-447.
57. Han, S. J.; Sun, Q. F.; Zheng, H. H.; Li, J. P.; Jin, C. D., Green and Facile Fabrication of Carbon Aerogels from Cellulose-Based Waste Newspaper for Solving Organic Pollution. *Carbohyd. Polym.* **2016,** *136*, 95-100.
58. Wang, L.; Cheng, J.; Kang, Q. S.; Wang, R.; Ruan, J. F.; Li, L. X.; Wu, L. X.; Li, Z. M.; Ai, N., Cobalt-Containing Nanoparticles Embedded in Flexible Carbon Aerogel for Spilled Oil Cleanup and Oxygen Reduction Reaction. *Compos. Part B-Eng.* **2019,** *174*, 107039.
59. Kong, B.; Tang, J.; Wu, Z. X.; Wei, J.; Wu, H.; Wang, Y. C.; Zheng, G. F.; Zhao, D. Y., Ultralight Mesoporous Magnetic Frameworks by Interfacial Assembly of Prussian Blue Nanocubes. *Angew. Chem. Int. Edit.* **2014,** *53*, 2888-2892.
60. Du, R.; Feng, Q. L.; Ren, H. Y.; Zhao, Q. C.; Gao, X.; Zhang, J., Hybrid-Dimensional Magnetic Microstructure Based 3d Substrates for Remote Controllable and Ultrafast Water Remediation. *J. Mater. Chem. A* **2016,** *4*, 938-943.
61. Kakunuri, M.; Wanasekara, N. D.; Sharma, C. S.; Khandelwal, M.; Eichhorn, S. J., Three-Dimensional Electrospun Micropatterned Cellulose Acetate Nanofiber Surfaces with Tunable Wettability. *J. Appl. Polym. Sci.* **2017,** *134*, 44709.
62. Duan, B.; Gao, H. M.; He, M.; Zhang, L. N., Hydrophobic Modification on Surface of Chitin Sponges for Highly Effective Separation of Oil. *ACS Appl. Mater. Inter.* **2014,** *6*, 19933-19942.
63. Ge, X.; Yang, W.; Wang, J.; Long, D. H.; Ling, L. C.; Qiao, W. M., Flexible Carbon Nanofiber Sponges for Highly Efficient and Recyclable Oil Absorption. *RSC Adv.* **2015,** *5*, 70025-70031.

64. Sun, H. Y.; Xu, Z.; Gao, C., Multifunctional, Ultra-Flyweight, Synergistically Assembled Carbon Aerogels. *Adv. Mater.* **2013,** *25*, 2554-2560.
65. Chen, L.; Du, R.; Zhang, J.; Yi, T., Density Controlled Oil Uptake and Beyond: From Carbon Nanotubes to Graphene Nanoribbon Aerogels. *J. Mater. Chem. A* **2015,** *3*, 20547-20553.
66. Yu, M.; Han, Y. Y.; Li, J.; Wang, L. J., Magnetic Carbon Aerogel Pyrolysis from Sodium Carboxymethyl Cellulose/Sodium Montmorillonite Composite Aerogel for Removal of Organic Contamination. *J. Porous Mater.* **2018,** *25*, 657-664.
67. Cao, X. J.; Zang, L. L.; Bu, Z. P.; Sun, L. G.; Guo, D. C.; Wang, C., Microfluidic Fabrication of Magnetic Porous Multi-Walled Carbon Nanotube Beads for Oil and Organic Solvent Adsorption. *J. Mater. Chem. A* **2016,** *4*, 10479-10485.

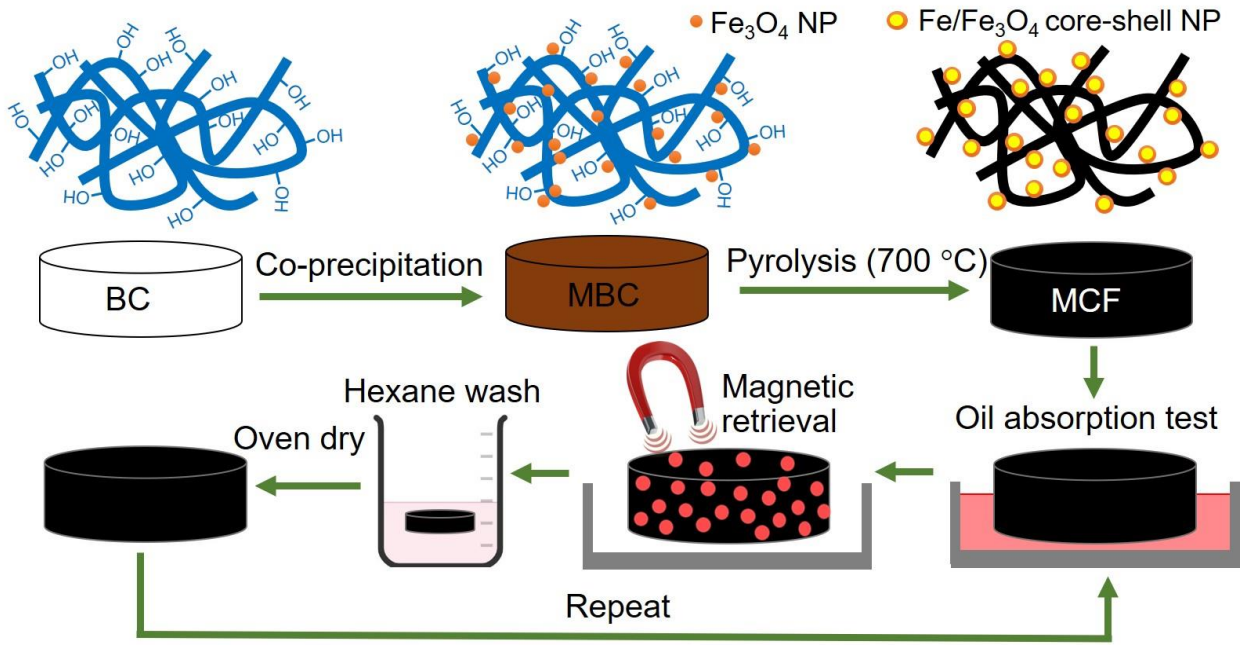


**Scheme 1.** A diagram for the synthesis of magnetic carbon fiber (MCF) aerogels and the oil absorption measurement.

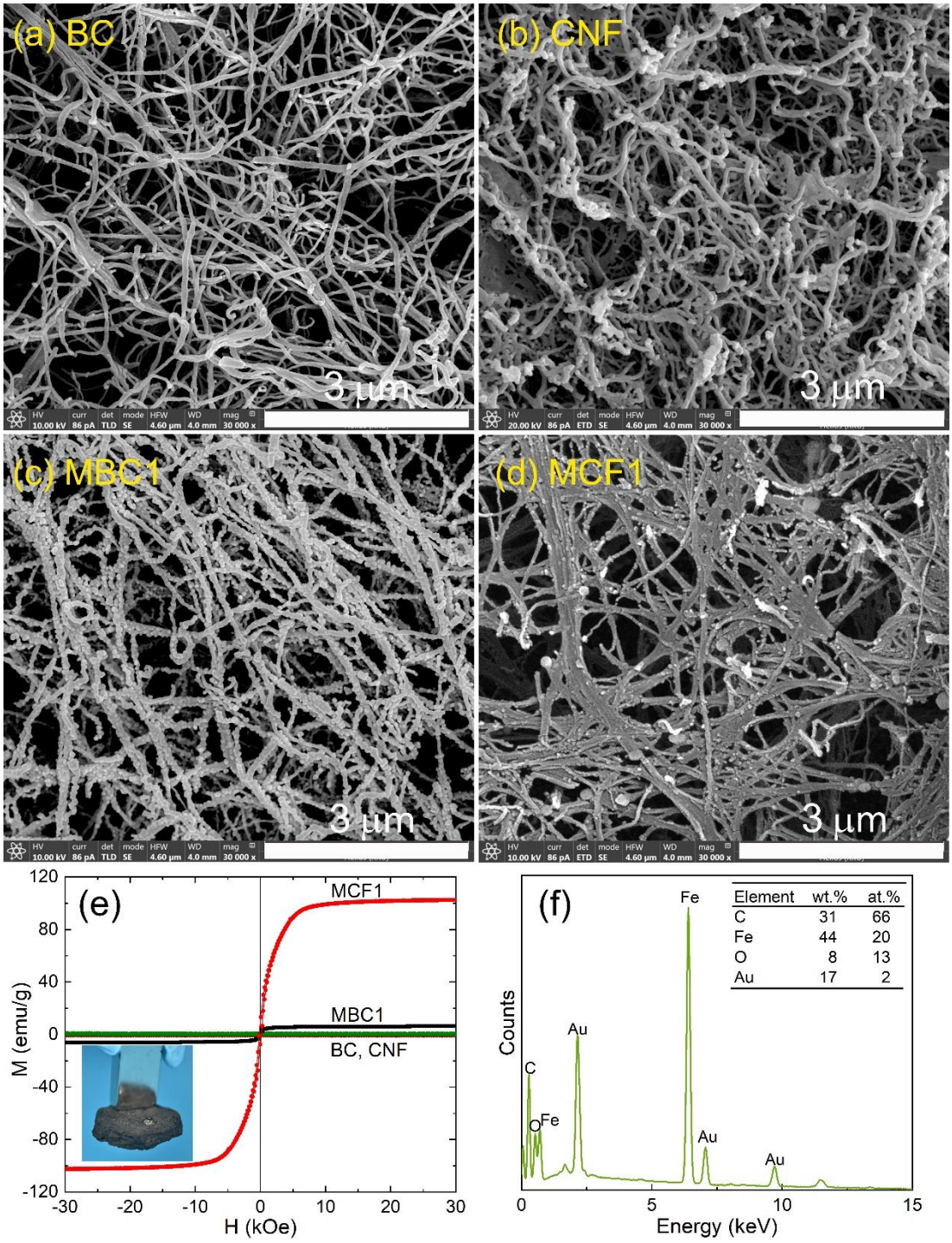


**Fig. 1.** Typical SEM micrographs of (a) BC, (b) CNF, (c) MBC1, (d) MCF1 aerogels. (e) Magnetization curves of the BC, CNF, MBC1 and MCF1 aerogels. (e: inset) the MCF1 aerogel magnetically elevated with a drop of water suspended on its surface. (f) EDS spectrum of the MCF1 aerogel.

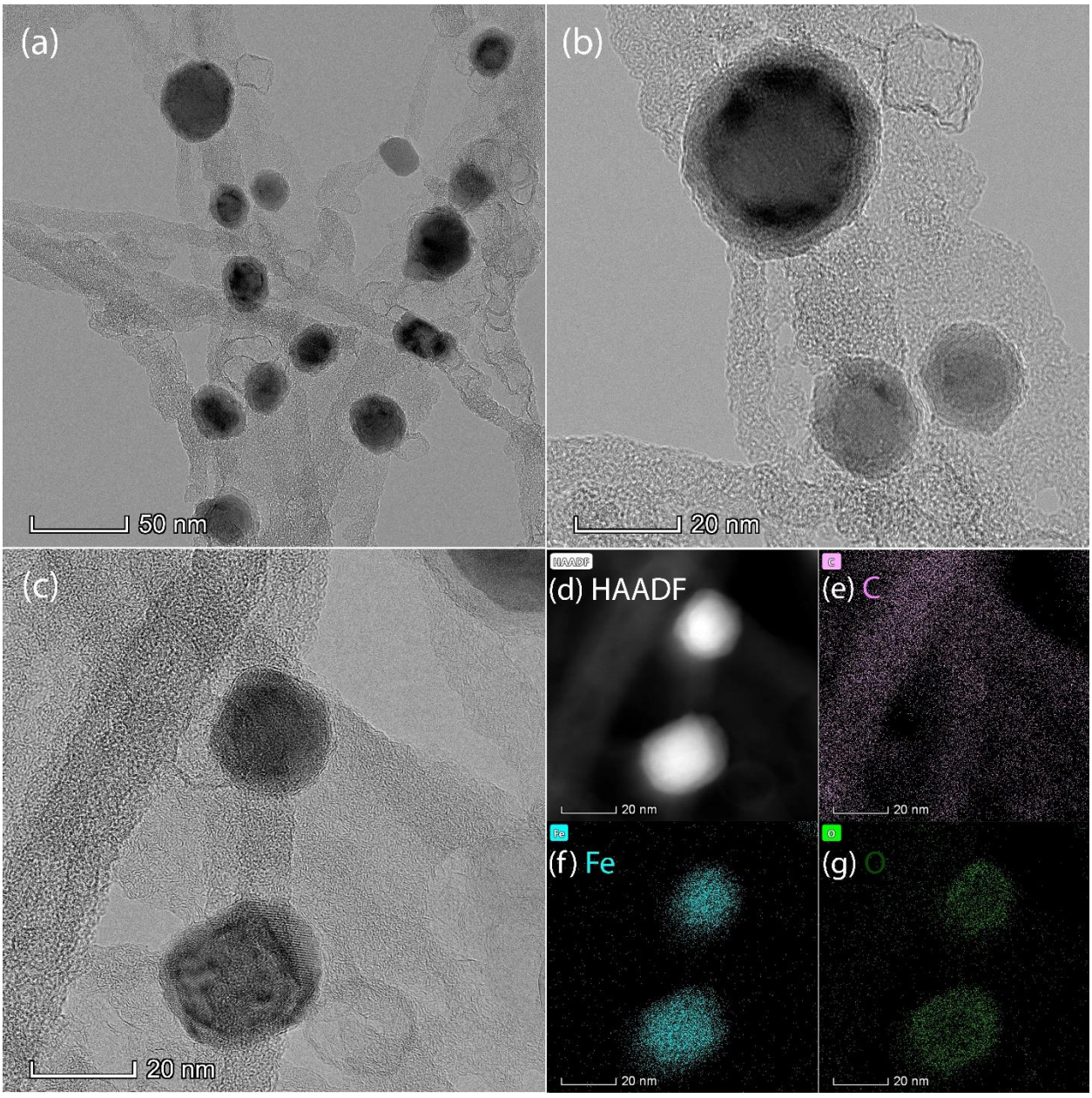


**Fig. 2.** (a)-(c) Typical TEM micrographs of the MCF1 aerogel showing the magnetic Fe/$Fe_3O_4$ core-shell nanoparticles anchoring on carbon nanofibers. (d) HAADF image, and the corresponding EDS mapping of the MNPs (e)-(g), revealing the enriched region of Fe and O in the centre and the outer surface, respectively.

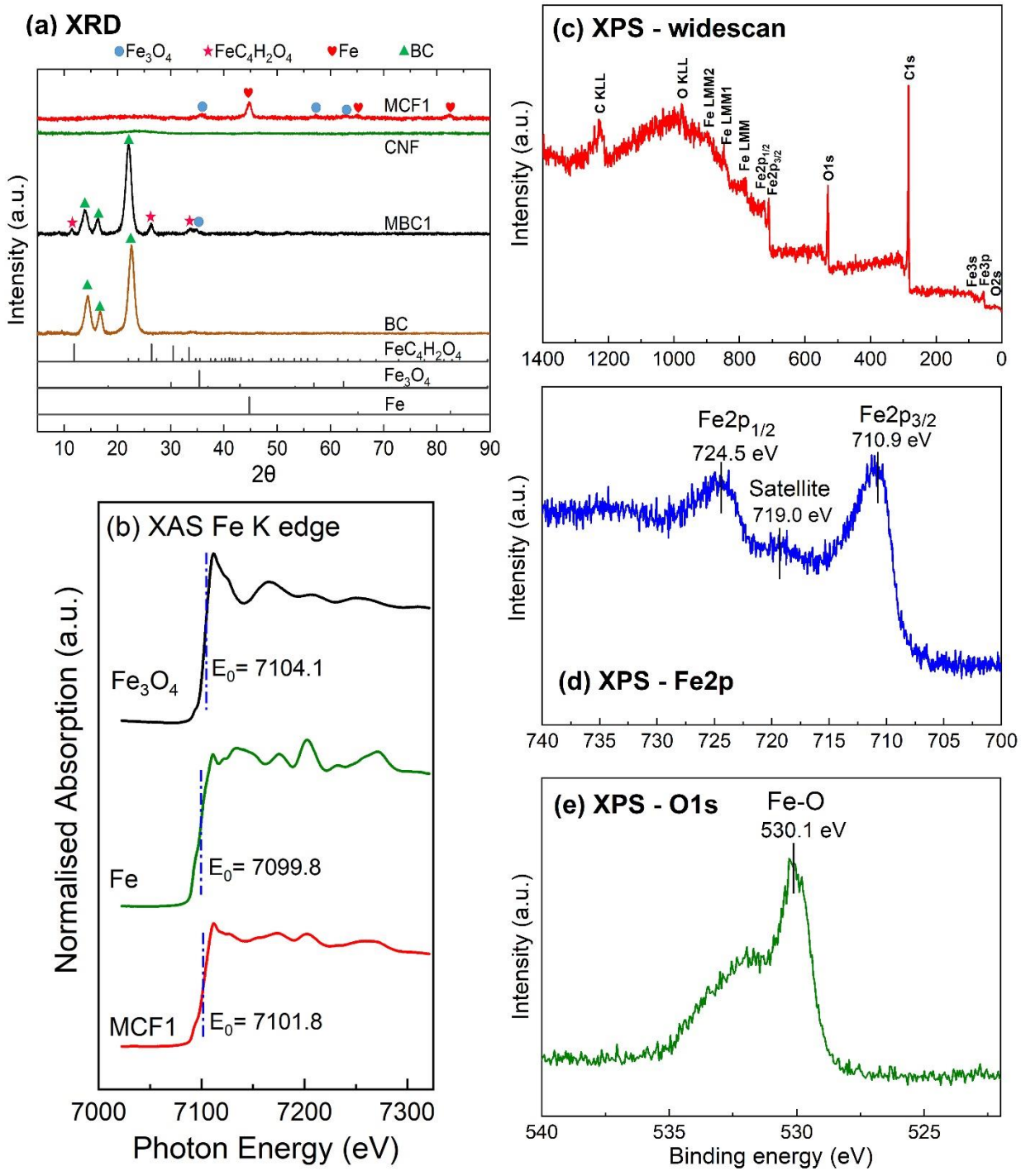


**Fig. 3.** (a) Typical XRD patterns of the BC, MBC1, CNF, and MCF1 aerogels, (b) XAS Fe K-edge energy of the MCF1 aerogel. (c)-(e) XPS spectra of the MCF1 aerogel.

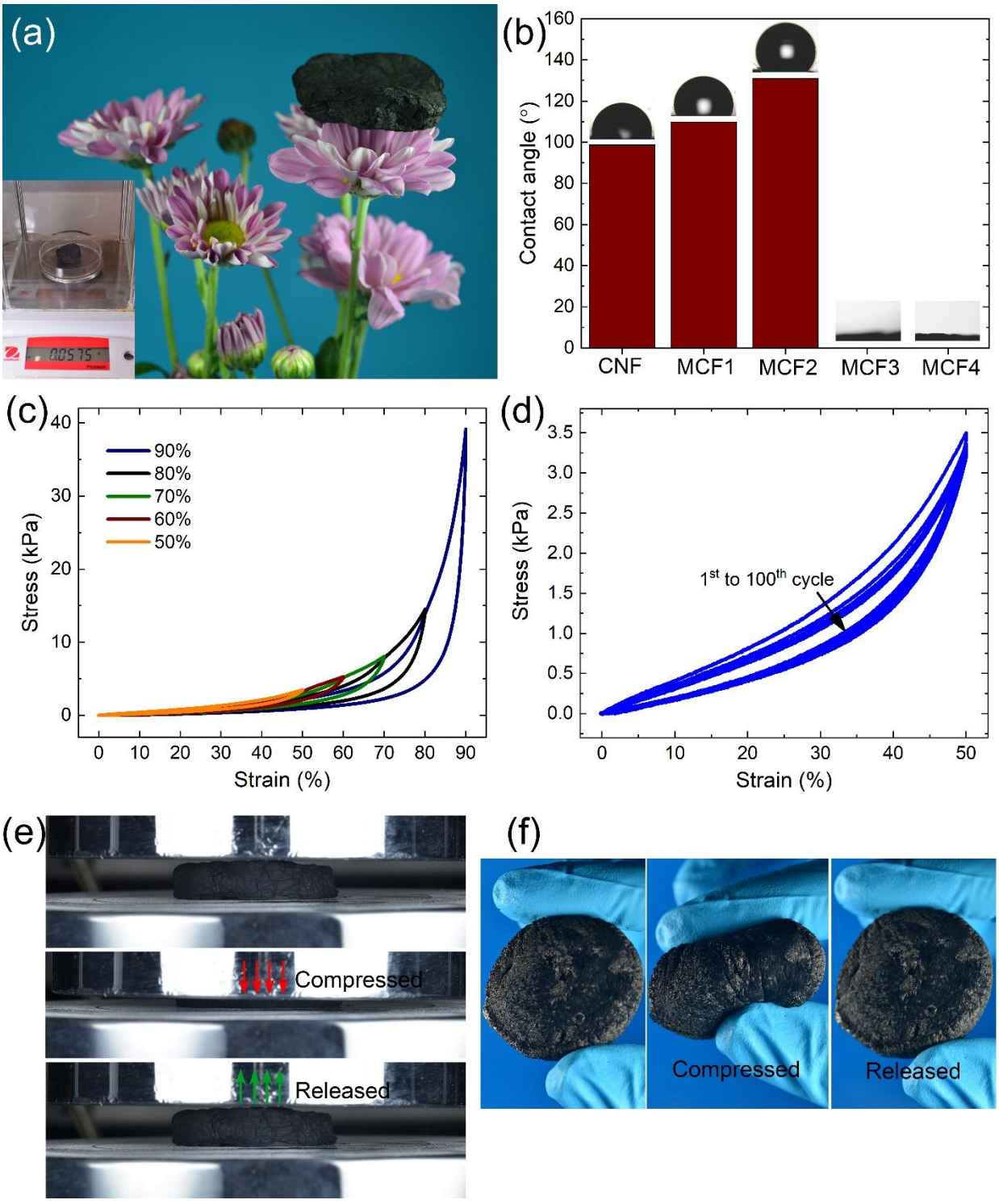


**Fig. 4.** (a) Demonstration of the ultralight weight of the MCF aerogel, (b) the water contact angle of the CNF and MCF aerogels, (c)-(d) compressive stress strain curves for the MCF1 aerogel, (e) the photographs showing the compressed MCF1 aerogel at 90% strain and the restoration after release, (f) the photographs of the MCF1 aerogel during squeezing from both sides.

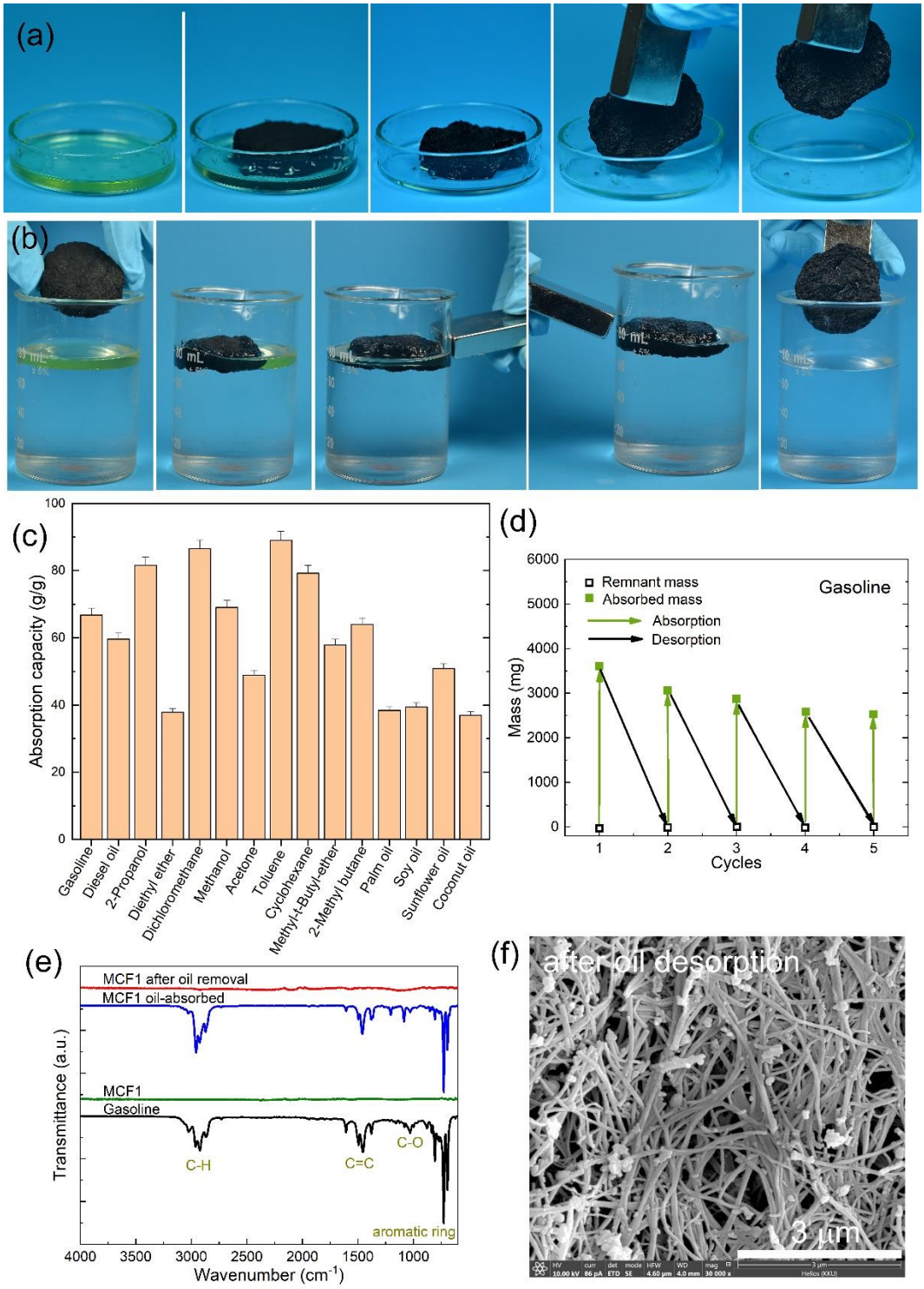


**Fig. 5.** (a) The absorption experiment and magnetic retrieval after oil absorption. (b) absorption of oil floating on water. A magnet was used for manipulation and retraction of the MCF aerogel. (c) the mass absorption capacity of the MCF1 aerogel over various types of oils/organic solvents. (d) The recyclability of the MCF aerogel by dissolution in hexane after oil absorption. (e) FTIR spectra of the MCF1 aerogel before, during, and after oil absorption. (f) SEM image of the MCF1 aerogel after oil desorption.

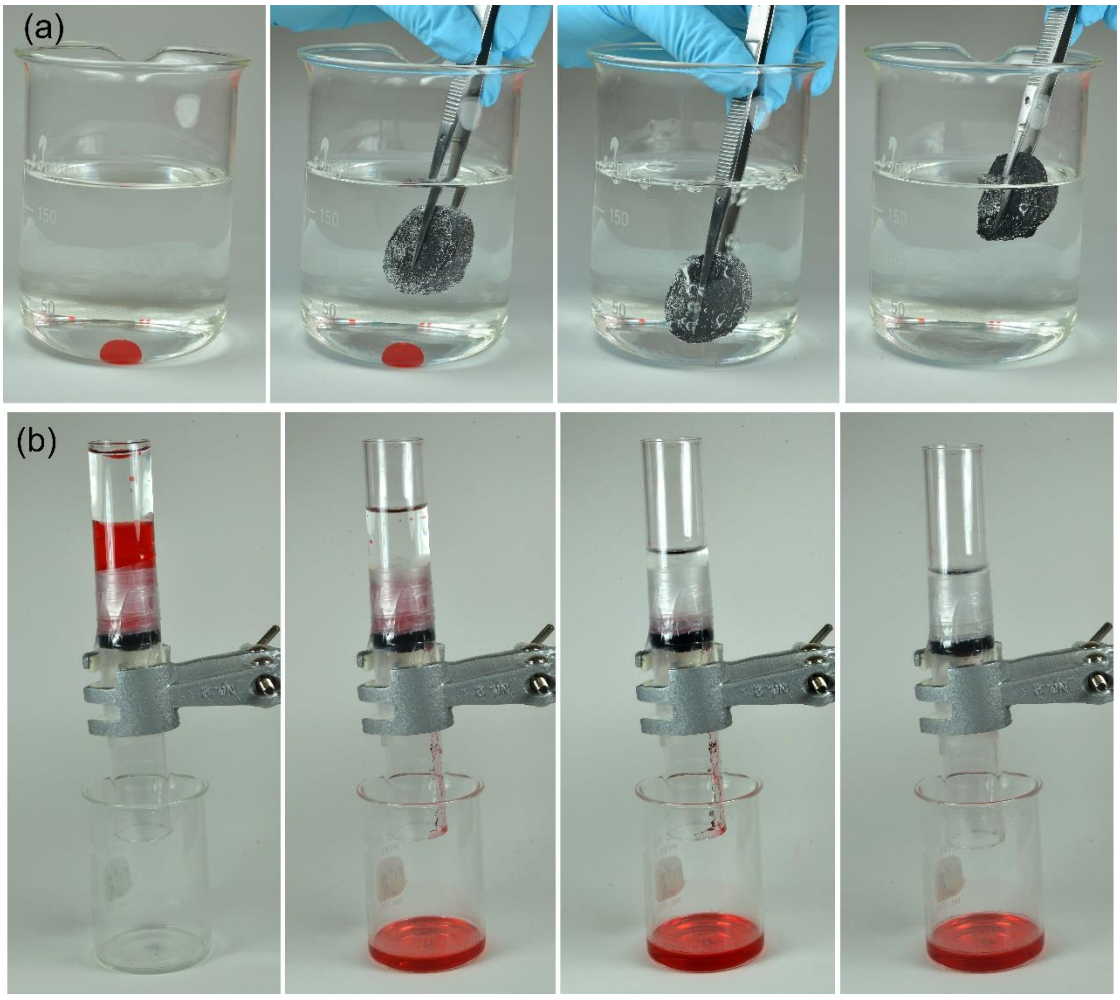


**Fig. 6.** Demonstration of (a) oil absorption under water, and (b) oil/water separation, for the MCF1 aerogel. The oil is dichloromethane-dyed with red color.

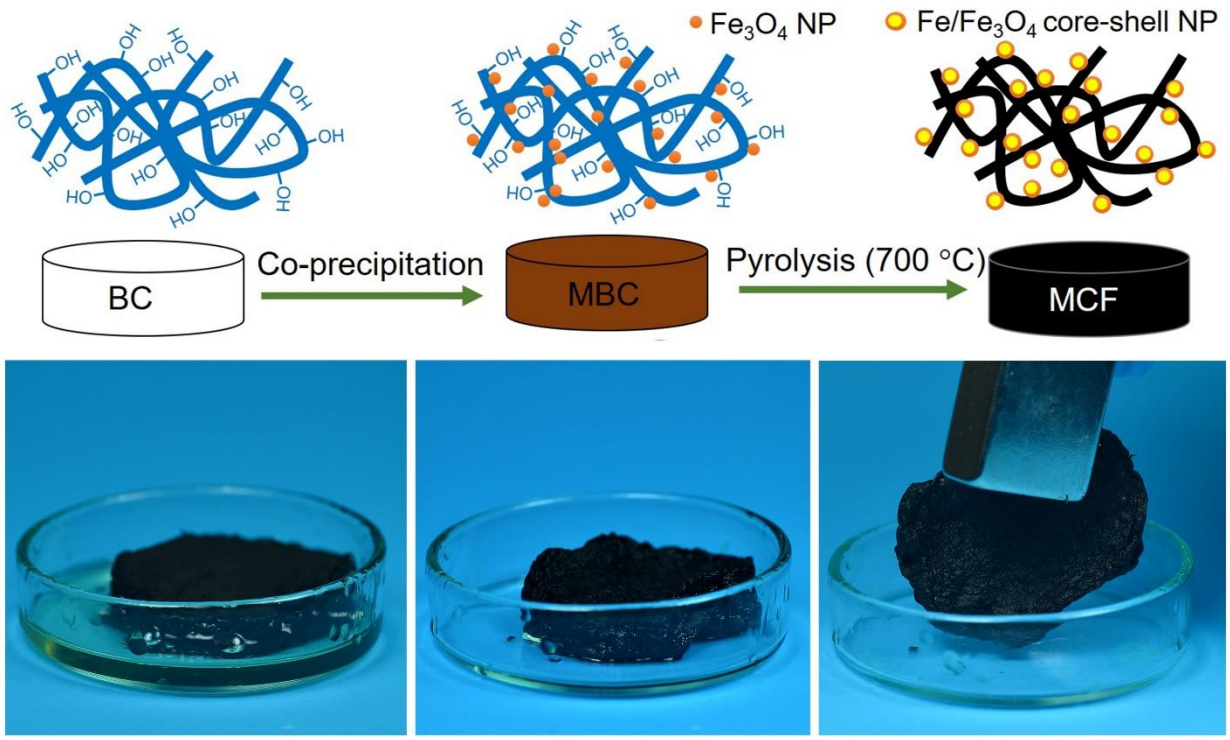


Table of Contents (TOC) graphics